6th International Conference on Multiphase Flow,
ICMF 2007, Leipzig, Germany, July 9 – 13, 2007

Evaluation of energy spectra in bubble driven liquid flows from direct numerical simulations

Milica Ilic[1], Martin Wörner[2] and Dan Gabriel Cacuci[3]

[1,2]Forschungszentrum Karlsruhe, Institute for Reactor Safety, Postfach 3640, 76021 Karlsruhe, Germany

[3]University of Karlsruhe, Institute for Nuclear Technology and Reactor Safety, 76131 Karlsruhe, Germany

E-mail: [1]ilic@irs.fzk.de, [2]woerner@irs.fzk.de, [3]cacuci@ikr.uni-karlsruhe.de

Keywords: bubble-induced turbulence, energy spectra, direct numerical simulation

Abstract

This paper deals with analysis of temporal velocity signals in bubble-driven liquid flows. The analysis are based on direct numerical simulations of mono-disperse bubbly flows in a confined vertical channel. Time histories of the liquid phase vertical velocity are used to evaluate autocorrelation functions and one-dimensional energy spectra at various spatial positions. Different methods proposed in literature for bridging over the gaps in the liquid velocity signal due to bubble passage are investigated. It has been found that the different methods have a significant influence on the energy of the spectrum, but also may result in a shift of the most energetic frequency.

1 Introduction

Despite the great technical importance of bubbly flows e.g. in nuclear and chemical engineering, several fundamental physical aspects are still not well understood. Examples are the generation of pseudo-turbulence by bubbles rising through otherwise stagnant liquid as it occurs e.g. in bubble columns and the interaction of bubbles with shear induced turbulence. A suitable measure to quantify bubble-induced pseudo turbulence or the modulation of shear induced turbulence by the presence of bubbles is the one dimensional power spectrum of the velocity fluctuations in the liquid phase.

One-dimensional spectra for bubbly air-water flow in grid generated turbulence were measured by Lance & Bataille (1991), who evaluated the spectra from velocity signals obtained by hot wire anemometry (HWA). They find that the classical -5/3 power law is progressively replaced by a -8/3 dependence at high frequencies and attribute this effect to the wakes of the bubbles. However, in recent HWA measurements of Rensen *et al.* (2005) this trend could not be confirmed. Rensen *et al.* (2005) find a more pronounced energy enhancement on small scales than on large scales owing to the presence of bubbles. This leads to a less steep slope in the spectrum as compared to the Kolmogorov -5/3 law. Rensen *et al.* (2005) attribute this discrepancy to different values of the bubblance parameter, which is defined as the ratio of the pseudo-turbulent contribution to the turbulence kinetic energy to that of the turbulence kinetic energy in the absence of bubbles. However, it appears that the bubblance parameter alone cannot explain the different spectral slopes observed in various experiments and there must be further parameters of influence.

Unfortunately, the evaluation of liquid phase turbulence spectra from experimental signals is associated with certain difficulties. In bubbly flows, the character of the hot wire signal is discontinuous due to the passage of bubbles. It is, therefore, necessary to adopt a specific signal processing in order to achieve a correct measurement of the liquid phase velocity. For velocity signals obtained by Laser Doppler Anemometry (LDA) the evaluation of turbulence power spectra is even more complicated (see Harteveld *et al.* (2005)). Due to the random distribution of the seeding particles, the signal is randomly sampled so that the standard Discrete Fourier Transform cannot be applied. A second complication especially at high void fraction and far from walls is that one of the two laser beams may be blocked so that no LDA measurement volume is created resulting in large gaps in the sampled data. Third, when the paths of the two laser beams are not blocked and a valid measurement volume is formed a bubble may cross the measurement volume itself resulting in difficulties to interpret the signal since at that moment - similar to HWA signals - the liquid velocity is not defined.

There exist several approaches how to bridge over the gap in the liquid velocity signal due to passage of a bubble. Tsuji & Morikawa (1982) replaced the defective parts of the signal by straight lines obtained by linear interpolation between the liquid signal parts. Gherson & Lykoudis (1984) suppressed the parts of the signal indicating the presence of the gas phase completely and patched together the successive liquid velocity records. Lance & Bataille (1991) replaced the characteristic function of the liquid phase by a sequence

of smoothing windows. Also Wang *et al.* (1990) replaced the gaps in the signal with the values of the mean liquid velocity. Panidis & Papailiou (2000) introduced an indirect analytic continuity which essentially presumes that the void fraction parts of the signal are filled with segments having the same statistical properties as those of the continuous phase velocity signal. Similar to Tsuji & Morikawa (1982), Rensen *et al.* (2005) and Luther *et al.* (2005) used a linear interpolation of the gaps when a bubble passes the hot wire sensor and estimated the power spectral density from a Fourier transform. They state that this approach to obtain the spectrum has to be used with caution, as it results in a frequency dependent bias. Instead, they show that for void fractions up to 2% autoregressive modelling can be used for estimation of the power spectral density and note that this method shows a negligible frequency dependent bias. Shawkat *et al.* (2007) investigated five different methods to replace the subsequent gaps in the signals and decided to use the linear interpolation technique.

In this paper temporal velocity "signals" from direct numerical simulations are used to investigate effects of different ways for bridging the gaps in velocity signals on the turbulence energy spectrum of the liquid phase. In particular, the methods of Gherson & Lykoudis (1984), Tsuji & Morikawa (1982), Wang *et al.* (1990) and Panidis & Papailiou (2000) are applied to DNS velocity data for the bubble driven liquid flow in a plane vertical channel. Therefore, in the investigated cases in the absence of bubbles there will not be any turbulent motion and as a consequence the bubblance parameter is infinite. Measurements of power spectra for the flow in bubble columns have been performed by Mudde *et al.* (1997), Ciu & Fan (2004)and Ciu & Fan (2005). In both cases the authors find a spectral slope of -5/3. However, in these experiments there exists a large scale liquid recirculation which is not present in the small scale computational domain with periodic boundary conditions considered in our numerical simulations.

In the remainder of the paper we first give a short description of our in-house computer code that is used to perform the direct numerical simulations of bubbly flows based on the volume-of-fluid method. Next we present the physical and numerical parameters of the simulations and discuss results for important mean and statistical quantities. In the main part of the paper we show characteristic time signals of the flow from which we compute the respective auto correlation function and power spectra using four different methods for replacing the gaps due to bubble passage.

2 Computation of bubble driven liquid flows by direct numerical simulations of bubble-array flows with computer code TURBIT-VoF

This section describes how the instantaneous data needed for the analysis of velocity fluctuations in bubble driven liquid flows have been obtained by direct numerical simulations of so-called bubble-array flows with the computer code TURBIT-VoF.

2.1 Mathematical formulation of gas-liquid flows in computer code TURBIT-VoF - an outline

TURBIT-VoF is an in-house computer code developed at the Institute for Reactor Safety in the Research Centre Karlsruhe for direct numerical simulations of dilute bubbly flows in plane channels. For the sake of consistency the mathematical formulation of gas-liquid flows applied in TURBIT-VoF is in the following briefly outlined. A detailed description of the code is given by Sabisch *et al.* (2001).

Using the local liquid volumetric fraction f to define mixture material properties such as density and viscosity:

$$\rho^* = f\rho_l^* + (1-f)\rho_g^* \quad \text{and} \quad \mu^* = f\mu_l^* + (1-f)\mu_g^*$$

and mixture flow properties such as centre-of-mass velocity and pressure:

$$\mathbf{u}^* = \frac{f\rho_l^*\mathbf{u}_l^* + (1-f)\rho_g^*\mathbf{u}_g^*}{f\rho_l^* + (1-f)\rho_g^*} \quad \text{and} \quad p^* = fp_l^* + (1-f)p_g^*$$

the behaviour of both phases, the liquid and the gas, as well as the dynamic boundary condition at the phase interface is in TURBIT-VoF described by the following single set of governing equations that express conservation of mass and momentum within the entire computational domain:

mass:

$$\nabla \cdot \mathbf{u} = 0 \tag{1}$$

momentum:

$$\frac{\partial \rho \mathbf{u}}{\partial t} + \nabla \cdot (\rho \mathbf{u}\mathbf{u}) = -\nabla p + \frac{1}{\mathrm{Re}_{\mathrm{ref}}} \nabla \cdot \mu(\nabla \mathbf{u} + \nabla \mathbf{u}^{\mathrm{T}}) - \frac{(1-f-\langle\alpha_g\rangle)\mathrm{E\ddot{o}}_{\mathrm{ref}}}{\mathrm{We}_{\mathrm{ref}}} \frac{\mathbf{g}^*}{|\mathbf{g}^*|} + \frac{\kappa a_i}{\mathrm{We}_{\mathrm{ref}}} \mathbf{n}. \tag{2}$$

where the following scaling applies:

$$\rho = \frac{\rho^*}{\rho_{\mathrm{ref}}} \quad \mu = \frac{\mu^*}{\mu_{\mathrm{ref}}} \quad \mathbf{x} = \frac{\mathbf{x}^*}{l_{\mathrm{ref}}} \quad \mathbf{u} = \frac{\mathbf{u}^*}{u_{\mathrm{ref}}} \quad t = \frac{t^* u_{\mathrm{ref}}}{l_{\mathrm{ref}}}$$

with the material properties of the liquid phase taken to be reference ones ($\rho_{\mathrm{ref}} = \rho_l^*$ and $\mu_{\mathrm{ref}} = \mu_l^*$) and the reference length, l_{ref}, and reference velocity, u_{ref}, to be specified. Note that dimensional quantities are denoted with the superscript *.

The reference Reynolds, Weber and Eötvos number are, respectively, given by:

$$\mathrm{Re}_{\mathrm{ref}} = \frac{\rho_l^* u_{\mathrm{ref}} l_{\mathrm{ref}}}{\mu_{\mathrm{ref}}} \quad \mathrm{We}_{\mathrm{ref}} = \frac{\rho_l^* u_{\mathrm{ref}}^2 l_{\mathrm{ref}}}{\sigma^*} \quad \mathrm{E\ddot{o}}_{\mathrm{ref}} = \frac{(\rho_l^* - \rho_g^*)|\mathbf{g}^*| l_{\mathrm{ref}}^2}{\sigma^*}$$

where σ^* stands for the surface tension and $\mathbf{g}^*$ represents the gravity, while subscripts l and g denote the liquid and the gas phase, respectively.

In order to prevent uniform downward acceleration of the whole system and to ensure by the same time a downward liquid flow in the vicinity of channel walls, an additional

body force, $\langle\rho^*\rangle\mathbf{g}^*/|\mathbf{g}^*|$, is imposed to both fluids, where $\langle\rho^*\rangle = \rho_l^* + \langle\alpha_g\rangle(\rho_g^* - \rho_l^*)$ represents the overall density of two-phase mixture. In relation to this, the dimensionless pressure is defined as:

$$p = (p^* - \rho_l^* \mathbf{g}\cdot\mathbf{x}^*)/(\rho_l^* u_{\text{ref}}^2)$$

while the buoyancy term in the momentum equation involves the overall gas volumetric fraction $\langle\alpha_g\rangle$.

The last term in the equation (2) expresses the contribution of the surface tension force where κ stands for twice the mean dimensionless interface curvature, $\mathbf{n}$ represents the unit normal vector at the phase interface pointing from the gas to the liquid phase and

$$a_i = l_{\text{ref}} a_i^*$$

represents dimensionless interfacial area concentration.

Employing the transport equation for the liquid volumetric fraction:

$$\frac{\partial f}{\partial t} + \mathbf{u}\cdot\nabla f = 0, \tag{3}$$

flow regions containing pure liquid (f=1) are distinguished from the pure gas ones (f=0). When $0 < f < 1$, an interface exists within the computational cell. In such cells the model of a homogeneous two-phase mixture is applied, where the equality of phase velocities and pressures is assumed.

Equations 1 and 2 are numerically integrated by a projection method where the resulting Poisson equation is solved by a conjugate gradient method. The time integration of the momentum equation is performed by an explicit third-order Runge-Kutta scheme. All spatial derivatives are approximated by second order central difference schemes. For solving the equation 3 a Volume-of-Fluid (VoF) procedure is applied. The interface orientation and location inside each mesh cell is reconstructed using PLIC (*P*iecewise *L*inear *I*nterface *C*alculation) method EPIRA which locally approximates the phase interface by a plane. The methodology is verified comparing numerical results with experimental data for the rise of an ellipsoidal bubble and an oblate ellipsoidal cap bubble (see Sabisch *et al.* (2001)).

2.2 Computational set-up for TURBIT-VoF simulations of bubble-array driven flows

The simulated flow pattern is named *bubble-array flow*. The term 'bubble-array flow' refers to a flow regime where monodisperse arrays of bubbles rise through otherwise stagnant liquid within a plane infinite channel. Such a flow pattern is in TURBIT-VoF represented by a fixed doubly periodic computational domain confined with two rigid walls (see Figure 1). The whole bubble-array flow can be imagined as a flow configuration where the bubble-array pattern presented in Figure 1 is periodically repeated in the vertical x_1 and span-wise x_2 direction. In relation to this, bubble-array flows simulated by TURBIT-VoF resemble in practice encountered developed gas-liquid flows within a flat bubble column with a moderate ratio of the bubble diameter to the column depth.

Two types of bubble-array flows are simulated: (i) *bubble-train flow* where only one bubble is suspended within the computational domain and (ii) *bubble-swarm flow* where the periodic cell contains a swarm of eight freely interacting bubbles. Although the developed flow regime in a flat bubble column is more realistically described by the concept of bubble-swarm than by the pattern of bubble-train flow, the latter simulation is performed to analyze effects of bubble population density on the liquid velocity fluctuations. The definition of the bubble-train configuration, namely, implies that all the bubbles within the whole channel are of an identical shape, move with the same velocity and are at constant distances from their neighbours. On the other side, the rise of an individual bubble in bubble-swarm flow is through the mutual interactions of bubble wakes influenced by the motion of other bubbles. Therefore, despite the same equivalent diameter, the bubbles within the bubble-swarm flow are, in principle, not of an identical shape and do not rise with the same velocity.

The computational domain for both simulations is specified to be a plane channel of the dimensionless size $l_1 = l_2 = l_3 = l = 1$. The domain is discretized with 64^3 uniform mesh cells for the simulation of the bubble-train flow. However, a numerical grid with the resolution of 100^3 turned out to be necessary in order to resolve the smallest eddies in the case of bubble-swarm flow. The equivalent bubble diameter, d_b, in both simulations is prescribed to be one fourth of the computational domain size. In relation to the aforementioned, the magnitude of overall gas volumetric fraction:

$$\langle\alpha_g\rangle = \frac{n_b d_b^3 \pi}{6 l^3}, \tag{4}$$

for the two simulated bubble-array flows differs only because of different number od bubbles contained within the computational domain n_b and not because of different geometrical parameters of the two flow configurations. Therefore, while in the case of bubble-train flow a very dilute bubbly flow with $\langle\alpha_g\rangle = 0.818\%$ is considered, with $\langle\alpha_g\rangle = 6.544\%$ the lower limit of a moderate bubbly flow is achieved in the bubble-swarm simulation.

Effects of physical parameters on the rise of gas bubbles are taken into account specifying the magnitude of bubble Eötvös number:

$$\text{Eö}_b = |\mathbf{g}^*| d_b^{*2} \frac{(\rho_l^* - \rho_g^*)}{\sigma^*} = 3.065 \tag{5}$$

and the magnitude of Morton number:

$$\text{M} = |\mathbf{g}^*| \mu_l^{*4} \frac{\rho_l^* - \rho_g^*}{\rho_l^{*2} \sigma^{*3}} = 3.06 \cdot 10^{-6}. \tag{6}$$

These values of Eötvös and Morton number are obtained adopting the following ratios of phase densities and phase viscosities:

$$\Gamma_\rho = \frac{\rho_g^*}{\rho_l^*} = 0.5 \;\text{ and }\; \Gamma_\mu = \frac{\mu_g^*}{\mu_l^*} = 1. \tag{7}$$

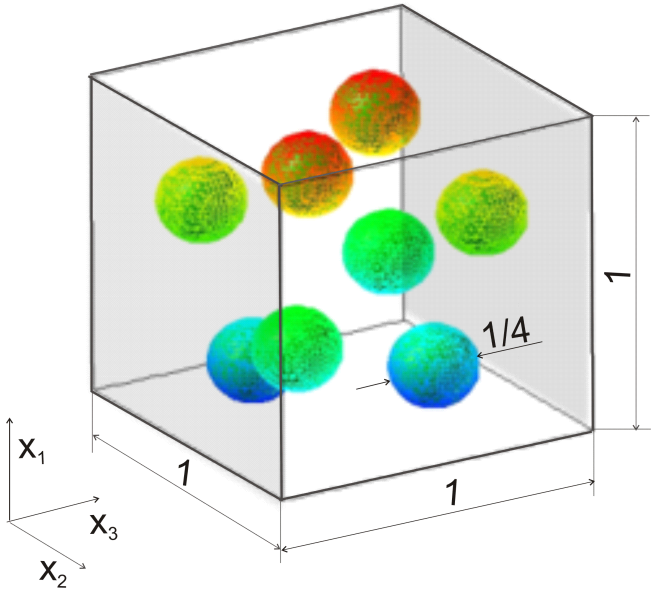

Figure 1: Computational domain for direct numerical simulations of bubble driven flows with TURBIT-VoF

The magnitude of the density ratio Γ_ρ may appear unusual and deserves some comments. The choice of this parameter was motivated by the results reported by Wörner (2003), who using TURBIT-VoF investigated the influence of the density ratio on the rise of a single ellipsoidal bubble with parameters $\mathrm{E\ddot{o}}_b = 3.065$, $\mathrm{M} = 3.06 \cdot 10^{-6}$ and $\Gamma_\mu = 1$. Comparing results of numerical simulations for Γ_ρ =0.5, 0.2, 0.1 and 0.02 he found that the phase density ratio, Γ_ρ, has a notable influence on the initial acceleration of the bubble, but does not affect the bubble shape and bubble Reynolds number when the bubble terminal velocity has been reached. Moreover, the liquid velocity scaled by the bubble rise velocity turned out to be virtually independent on Γ_ρ in the steady flow regime.

The bubble-train flow is computed starting from an initial situation where one spherical bubble is positioned in the centre of the channel filled with stagnant liquid. Using time step width of $\Delta t = 10^{-4}$ in total 60 000 time steps are computed. In the simulation of the bubble-swarm flow 8 spherical bubbles are placed inside the quiescent liquid and arranged by slight perturbations of a regular pattern in each coordinate direction as it is presented in Figure 1. Due to higher bubble-induced agitation of the liquid flow the magnitude of time step width of $\Delta t = 0.5 \cdot 10^{-4}$ has been necessary. In total 120 000 time steps are computed.

For an easy reference the computational set-up of the performed simulations is presented in Table 1.

Table 1: Computational set-up specified in DNS of bubble-array flows with code TURBIT-VoF

type of bubble-array flow	bubble-train	bubble-swarm
reference length	4m	4m
reference velocity	1m/s	1m/s
computational domain size[a]	1x1x1	1x1x1
number of grid points	64^3	100^3
width of grid cell	0.015625	0.01
bubble equivalent diameter[a]	0.25	0.25
number of bubbles	1	8
overall gas volume fraction	0.818%	6.544%
phase density ratio	0.5	0.5
phase viscosity ratio	1	1
Morton number	$3.06 \cdot 10^{-6}$	$3.06 \cdot 10^{-6}$
bubble Eötvös number	3.065	3.065
reference Eötvös number	49.05	49.05
reference Weber number	2.5	2.5
reference Reynolds number	100	100
initial conditions	stagnant	stagnant
time step width[a]	10^{-4}	$0.5 \cdot 10^{-4}$
number of time steps	$0.6 \cdot 10^4$	$1.2 \cdot 10^4$
computed time [a]	6	6

[a] dimensionless

3 Analysis of computed three-dimensional motion of bubble-arrays

Our intuition suggests that the bubble-induced velocity fluctuations of the liquid phase are strongly related to the the dynamics of bubbles. This is, particulary, expected in bubble-swarm flows where, owing to the proximity of other bubbles, the motion of an individual bubble is more complex. In this context, this section presents a detailed analysis of three-dimensional bubble-array evolution for the simulated cases.

An overall impression on bubble-array dynamics as well as characteristics of bubble shape and orientation are obtained through flow visualisation by use of AVS software. A detailed analysis of individual bubble motion is performed by evaluation of bubble trajectories and bubble rise velocities.

The position of centre-of-mass of the m^{th} bubble[1] at time instant t is evaluated by:

$$\mathbf{r}_b^m = \frac{\int_{V_b^m} \mathbf{r}\mathrm{Ind}(\mathbf{r})dV}{\int_{V_b^m} \mathrm{Ind}(\mathbf{r})dV}, \qquad (8)$$

where V_b^m represents volume of the m^{th} bubble and dV is the volume of mesh cell. In order to avoid an interference of individual bubbles within the bubble-swarm, cells belonging to a certain bubble are marked introducing a bubble indicator function, $\mathrm{Ind}(\mathbf{r})$. This function is defined to have a zero value if the considered cell is fully occupied with the liquid phase and a constant value m if the cell is a part of the bubble with the ordinal number m.

[1]The notation used in the presentation of the applied methodology concerns more general case of the bubble-swarm flow where an individual bubble within the considered swarm of bubbles is associated with its ordinal number m ($m = 1, n_b$). To apply corresponding formulae on the case of the bubble-train flow one should simply put $m = 1$.

The velocity of the bubble centroid is evaluated either by:

$$\mathbf{u}_b^m = \frac{\int_{V_b^m} \mathbf{u}\mathrm{Ind}(\mathbf{r})dV}{\int_{V_b^m} \mathrm{Ind}(\mathbf{r})dV}, \tag{9}$$

where $\mathbf{u}$ represents the velocity computed by TURBIT-VoF, or differentiating the bubble path:

$$\mathbf{u}_b^m = \frac{d\mathbf{r}_b^m}{dt}. \tag{10}$$

It has been verified numerically that these two formulae give identical results. The former is used for the initial time step ($t = 0$), while the latter is applied when positions of the bubble centroid are known for two subsequent time steps ($t > 0$). The rise velocity of the swarm is computed as the arithmetic mean of the individual bubble rise velocities.

Bubble shape and liquid phase velocities at chosen span-wise position are for both bubble-array flows visualized in Figure 2. In the case of bubble-train flow an axisymmetric ellipsoidal bubble shape can be observed with the major axis parallel to the horizontal plane and with the axis aspect ratio $\kappa = 1.555$. In the bubble-swarm flow bubbles also took an ellipsoidal shape, but with major axis not perfectly aligned with the horizontal plane and with some slight differences in the shape of individual bubbles. Considering these differences as negligible, an average ellipsoid axis aspect ratio of $\kappa = 1.526$ can be estimated, what is $\approx 2\%$ lower value than in the case of bubble-train flow. The differences in the bubble shape between the two simulated bubble-array flows may, therefore, be neglected. However, when agitation of the liquid phase by rising bubbles is put into consideration, striking differences between the bubble-train and bubble-swarm flow can be observed. While in the bubble-train flow, namely, an intensive upward motion of the liquid phase is, through the bubble rise, induced only in the central part of the channel, perturbations of the liquid phase generated through the bubble-induced displacement of the liquid as well as through the mutual interaction of bubble wakes are in the case of bubble-swarm flow evident in the whole channel.

The trajectory of the bubble-train may be considered as an approximatively straight path taking into account that during the whole simulation time an individual bubble within the array vertically rose a distance of $\approx 19l$ with the maximal lateral deviation of its trajectory of less than $0.05l$. Therefore, it can be concluded that the chosen flow configuration ensures that neither laterally neighbouring bubble-arrays nor channel walls influence the shape of the bubble-train rising path. On the other side, Figure 3 shows that in bubble-swarm flow significant movements of individual bubbles occur in both, wall-normal and span-wise, directions. These lateral movements of bubbles in the bubble-swarm scenario lead to the formation of two bubble populations approximatively aligned with channel walls. It has also been observed that the tendency to horizontal alignment of bubbles, known as bubble rafting, is suppressed by repelling effects of bubble wakes that occur after a certain bubble approached the other one beyond a critical distance.

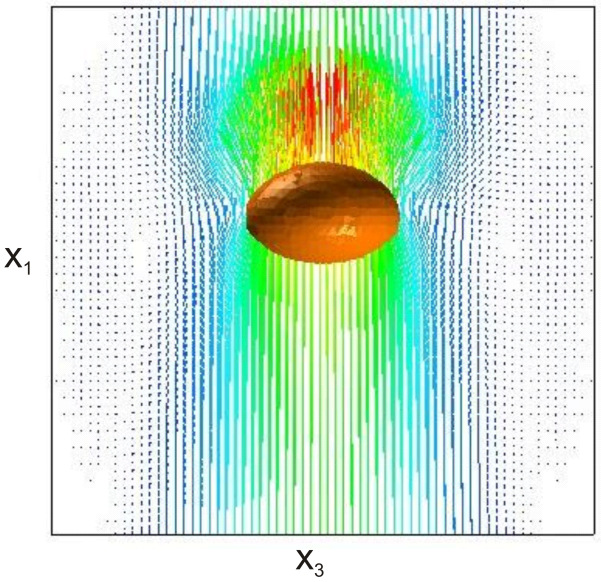

(a) bubble-train at $t = 5.5$ with liquid flow at $x_2 = 0.5$

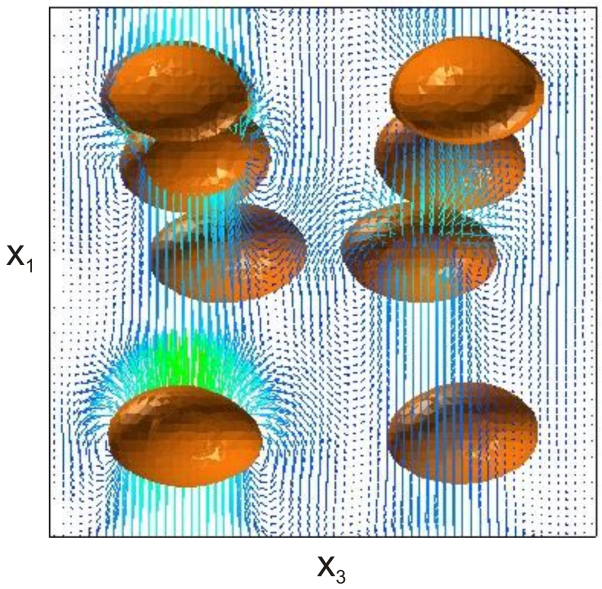

(b) bubble-swarm at $t = 5.5$ with liquid flow at $x_2 = 0.25$

Figure 2: Visualization of computed bubble-array flows

Further information about the rise of bubble-arrays with different number of bubbles can be drawn from Figure 4, where the time evolution of the rise velocities for the entire bubble-arrays as well as of the individual bubbles within the bubble-swarm is presented. It is evident that, except for a short initial phase of simulation, the acceleration of the bubble-train is stronger than the one of the bubble-swarm. Such a behaviour is caused by the larger drag due to increased vorticity deposition in the case of thicker bubble population. Even though the individual bubble motion shows the transient behaviour owing to mutual bubble wake interactions, the whole swarm of bubbles reaches a well defined steady state quite quickly. The magnitudes of the

rise velocities estimated for the steady-state regime for the bubble-train, bubble-swarm and individual bubbles within the bubble swarms are presented in Table 2.

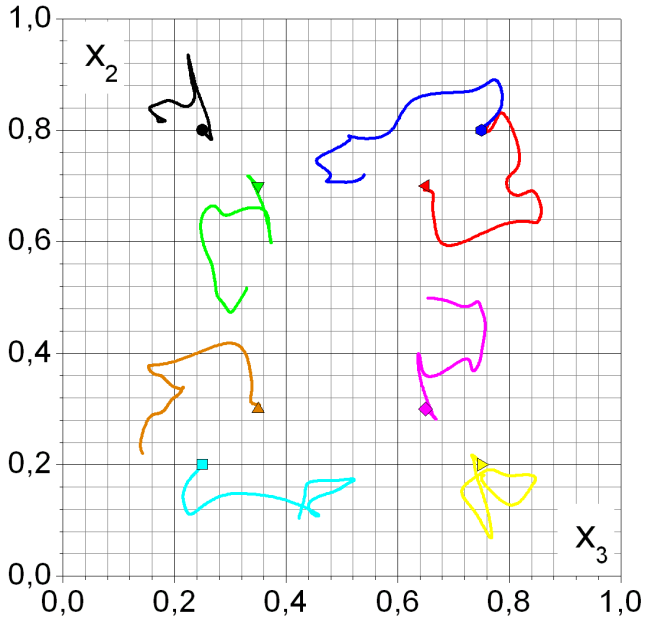

Figure 3: Lateral movements of individual bubbles computed in bubble-swarm flow scenario. Symbols represent initial bubble positions.

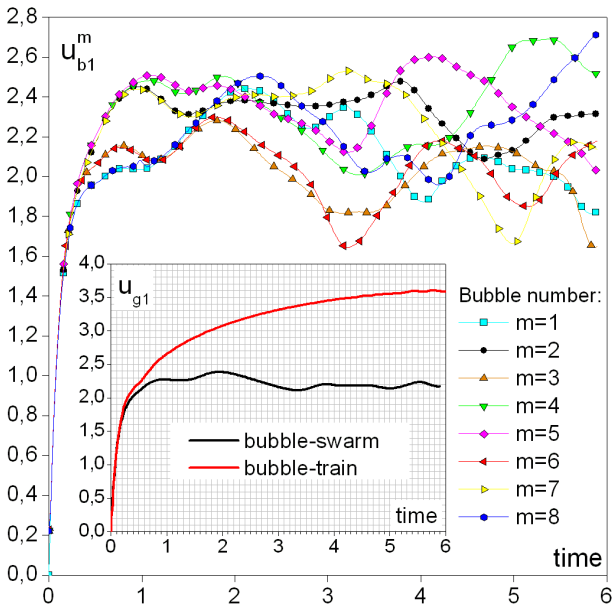

Figure 4: Time evolution of the rise velocity of individual bubbles in bubble-swarm flow scenario (bubble notation is compatible with Figure 3). Mean velocities of the bubble-train and the bubble-swarm as the whole are presented in subfigure.

Table 2: List of main parameters describing three-dimensional motion of computed bubble-arrays

type of bubble-array	bubble-train	bubble-swarm
rise length [a c]	19.10	13.31
lateral bubble motion[c]	negligible	strong
mean bubble rise velocity [a b]	3.586	2.218
mean bubble Reynolds number [b]	89.65	55.45
bubble axis aspect ratio [b]	1.555	1.535

[a] dimensionless
[b] in steady state
[c] during the whole simulation period

4 Analysis of time signals computed by direct numerical simulations of bubble-array flows

A storage of DNS data for each computed time instant and over the whole computational domain requires a huge memory space. For that reason the complete data sets are stored only for certain time intervals (typically every 250^{th} time step). A record of instantaneous velocity components and local liquid volumetric fraction necessary for an analysis of time signals are sampled at every time step of integration only for specified coordinate positions. In here presented simulations of bubble-array flows temporal records of instantaneous quantities (hereafter called time signals) are stored for one wall-normal bar of cells ($x_1 = 0.5$, $x_2 = 0.5$ and $x_3 = 0 - 1$) in the case of bubble-train flow and for one bar of cells parallel to the wall ($x_1 = 0.5$, $x_2 = 0 - 1$ and $x_3 = 0.25$) in the case of bubble-swarm flow. In Figure 5 and Figure 6 examples of computed time signals are presented for bubble-train and bubble-swarm flow, respectively.

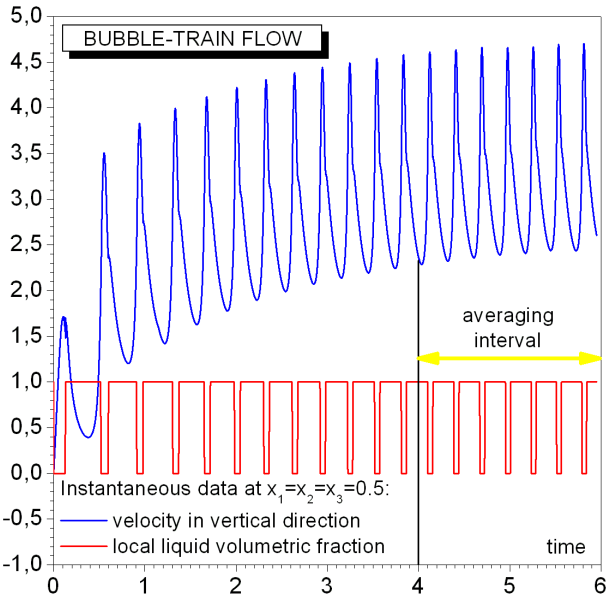

Figure 5: Time signals computed by DNS of bubble-train flow.

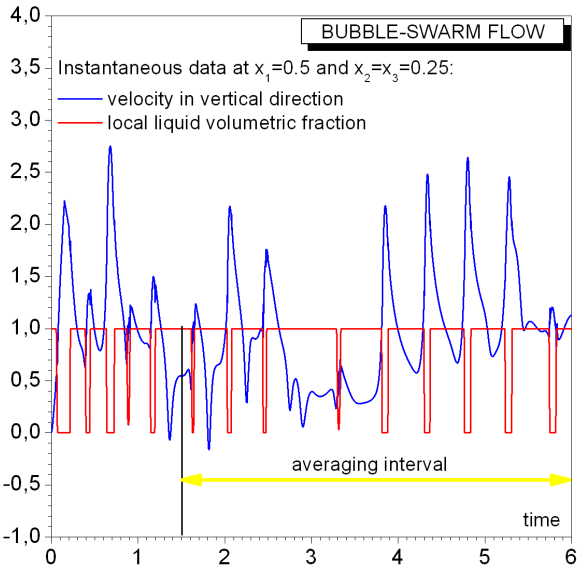

h

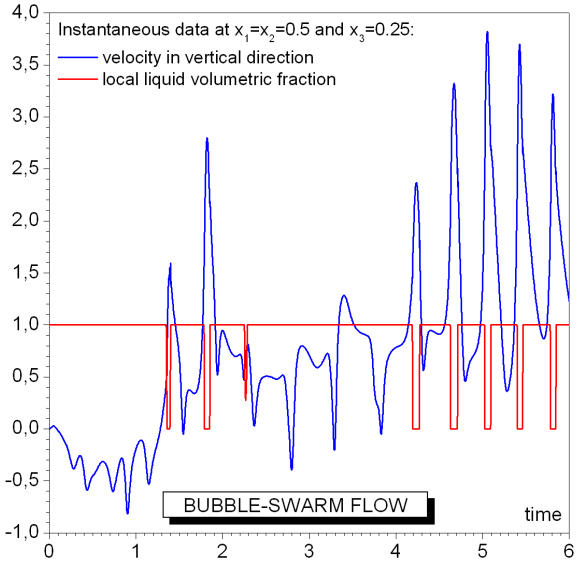

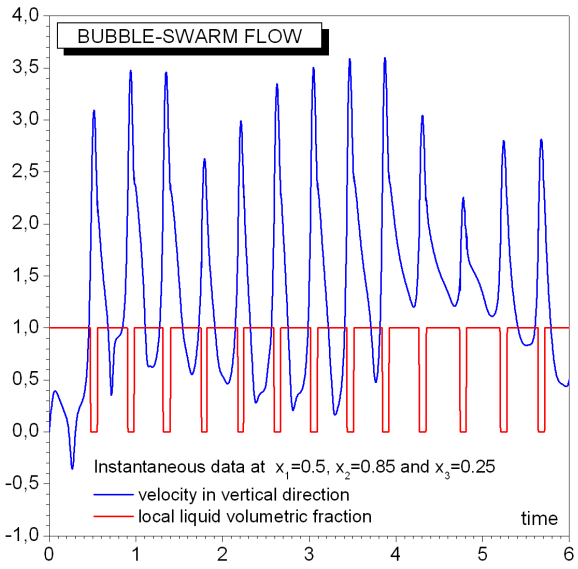

Figure 6: Time signals at different positions computed by DNS of bubble-swarm flow.

DNSs give time signals for the velocity of the two-phase mixture. In order to extract time steps in which the considered mesh cell is filled with pure liquid, the indicator function of the liquid phase is defined as:

$$\phi_l(t) = 1 \;\text{ if }\; f(t) = 1 \qquad (11)$$
$$= 0 \;\text{ otherwise,}$$

where $f(t)$ is the local liquid volumetric fraction computed by TURBIT-VoF simulations in considered mesh cell at the time instant t. The averaging of phase indicator function gives mean liquid volumetric fraction:

$$\alpha_l = \frac{1}{t_e - t_s} \sum_{t_s}^{t_e} \phi_l(t) \Delta t, \qquad (12)$$

where t_s and t_e are the lower and the upper limit of the averaging interval.

Eliminating all but the data for the liquid phase, the gaps in time velocity signals are produced. In relation to this, liquid velocity is not a field quantity as it is not defined at all time domains under consideration. Kataoka & Serizawa (1989) have, however, shown that the quantity $\phi_l \mathbf{u}_l$ is a field quantity and that so-called phase-weighted averaging of intermittent liquid velocity signals can be performed as:

$$\overline{\overline{u}}_{li} = \frac{1}{(t_e - t_s)\alpha_l} \sum_{t_s}^{t_e} u_{li}(t)\phi_l(t) \cdot \Delta t, \qquad (13)$$

where i denotes coordinate direction ($i = 1, 2, 3$).

The averaging of time signals is in this analysis done starting from the time instant $t_s = 4$ in the case of bubble-train and from $t_s = 1.5$ in the bubble-swarm scenario. In both cases the averaging is performed up to the time instant $t_e = 6$. Obtained profiles of mean liquid velocities and mean liquid volumetric fraction are presented in Figure 7a for bubble-train and Figure 7b for bubble-swarm flow.

Fluctuating parts of liquid phase velocity evaluated as:

$$u_{li}^{'}(t) = u_{li}(t) - \overline{\overline{u}}_{li}, \qquad (14)$$

are also not field quantities. However, when they are multiplied with $\phi_l(t)$ their averaging can be performed in an analogous way as it is done by equation (13). Due to their relevancy, the formulations of root-mean-square value of liquid velocity fluctuations in the vertical direction:

$$u_{l1rms} = \sqrt{\frac{1}{(t_e - t_s)\alpha_l} \sum_{t_s}^{t_e} u_{l1}^{'}(t) u_{l1}^{'}(t) \phi_l(t) \Delta t}, \qquad (15)$$

and turbulence kinetic energy of the liquid phase:

$$k_l = \frac{1}{2} \frac{1}{(t_e - t_s)\alpha_l} \sum_{t_s}^{t_e} u_{li}^{'}(t) u_{li}^{'}(t) \phi_l(t) \Delta t \qquad (16)$$

are here given (in equation (16) summation over the indice i applies). Profiles of u_{l1rms} and k_l computed for investigated bubble-array flows are presented in Figure 8.

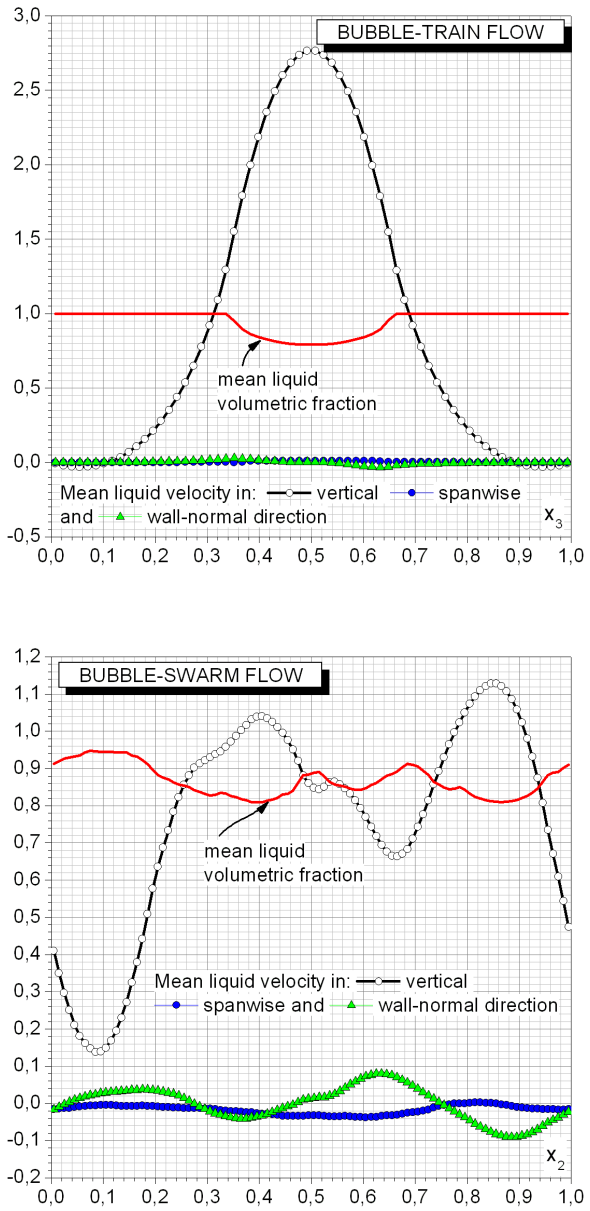

Figure 7: Profiles of mean quantities in bubble-array flows.

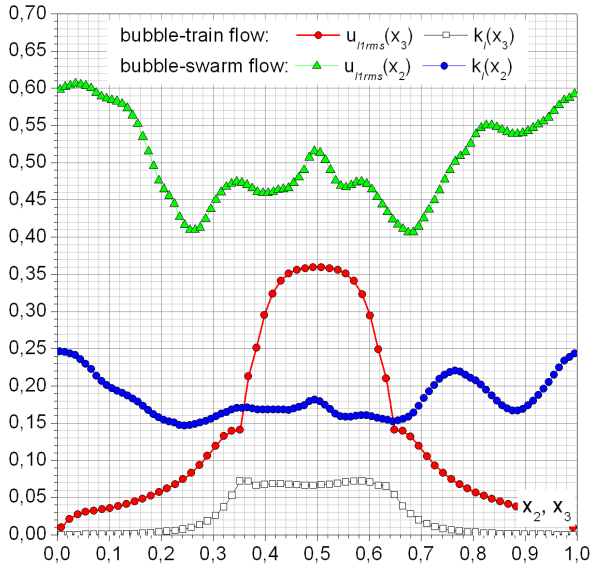

Figure 8: Profiles of turbulence quantities in bubble-array flows.

5 Evaluation of autocorrelation function from temporal velocity signals computed by direct numerical simulations of bubble-array flows

While the liquid phase indicator function ϕ_l is sufficient to determine liquid phase averaged quantities, a residual problem has to be solved when autocorrelation function of liquid velocity fluctuations is considered. The main difficulty encountered when the autocorrelation function in bubbly two-phase flow is computed, is that the liquid velocity signal is frequently interrupted by bubble passages. This discontinuous character of the signal makes it necessary to adopt a specific signal processing. In this section four different methodologies are applied to evaluate autocorrelation function of liquid velocity fluctuations in stream-wise direction (x_1) from aforementioned temporal velocity signals computed by DNS of bubble-array flows.

Currently, there are two approaches how to formulate the autocorrelation function in bubbly flows.

Tsuji & Morikawa (1982), Gherson & Lykoudis (1984) and Wang *et al.* (1990) apply the following single-phase formulation of the autocorrelation function at time lag $l\Delta t$:

$$R_{11}(l\Delta t) = \frac{1}{N-l} \sum_{n=1}^{n=N-l} u'_{l1,n} u'_{l1,n+l}, \qquad (17)$$

and propose different methods for bridging over missing parts of the signal. Gherson & Lykoudis (1984) suppress parts of the signal concerning gas phase and patch corresponding liquid velocity records. Wang *et al.* (1990) apply so-called rectangular window technique, which assumes that the parts of the signal indicating the gas phase velocity may be replaced by the mean velocity of the liquid phase. Tsuji & Morikawa (1982) analyzed possibilities for replacement of the defective parts of the signal by suitable lines. They tested three possible ways of interpolation: (i) to hold the liquid velocity value before the defect, (ii) to adopt zero value of velocity in periods of bubble passages and (iii) to replace the gaps by straight lines connecting regular parts. The authors recommended the third way as the most suitable method of signal processing in bubbly flows.

Different to the aforementioned approaches, Panidis & Papailiou (2000) formulated an autocorrelation function, which essentially presumes that the gas portion of the signal is filled with segments having the same statistical properties as those of the liquid velocity signal. An advantage of this assumption is that the reconstruction of the missing parts of the signal is not required. The authors started from the equation (17) and assumed that the elimination of some of the products of the autocorrelation function using a random function m (which

has the value 1 for the remaining parts and 0 for those to be eliminated) will not alter the probability density function and that the mean value can be estimated as:

$$R_{11}(l\Delta t) = \frac{1}{\sum_{n=1}^{n=N-l} m_n} \sum_{n=1}^{n=N-l} m_n u'_{l1,n} u'_{l1,n+l}, \quad (18)$$

where m_n $(n = 1..N)$ for the case of time signals obtained by direct numerical simulations can simply be estimated from phase indicator function:

$$m_n = \phi_n \phi_{n+l}, \quad (19)$$

since no biased effects are introduced.

The autocorrelation functions evaluated applying the aforementioned methods are compared in Figure 9 for the case of bubble-train flow and in Figure 10 for bubble-swarm flow. It is noted that respective autocorrelation functions are evaluated at the positions for which time signals are presented in Figure 5 and Figure 6. To provide a better comparison of the autocorrelation functions at the three positions in bubble-swarm flow, in Figure 10 the same range has been chosen for the ordinate.

Figure 9 and Figure 10 show (i) that the graph of the autocorrelation function obtained applying the method of Gherson & Lykoudis (1984) is shifted with respect to the graphs of the other three methods (for the discussion of this topic see the next section) and (ii) that R_{11} magnitudes evaluated by the aforementioned approaches significantly differ. As an estimate od the performance of the considered methods in Table 3 the magnitudes of the autocorrelation functions at zero time lag are compared with the rms value od the liquid velocity fluctuations evaluated on the basis of its exact formulation (see equation 15).

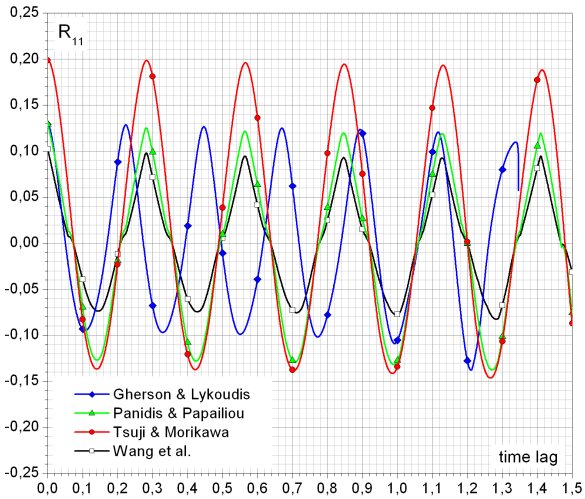

Figure 9: Autocorrelation functions evaluated for bubble-train flow using different methods for signal processing of temporal liquid velocity signals.

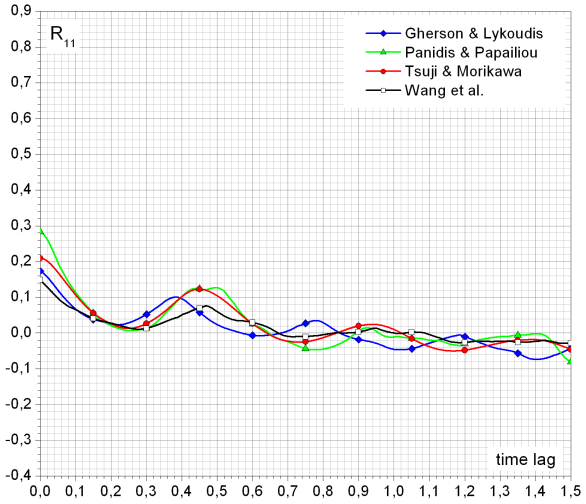

(a) $x_1 = 0.5$, $x_2 = 0.25$ and $x_3 = 0.25$

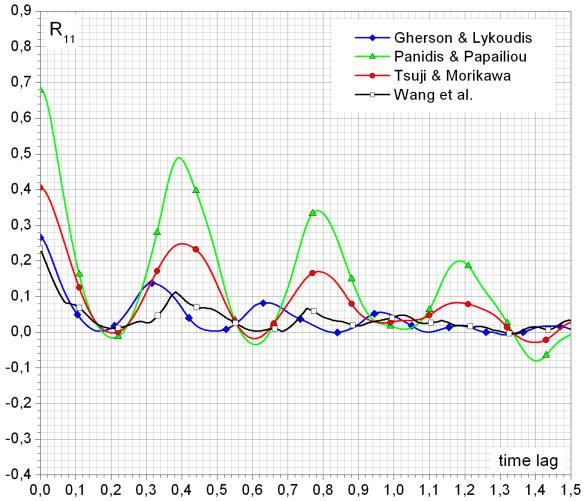

(b) $x_1 = 0.5$, $x_2 = 0.5$ and $x_3 = 0.25$

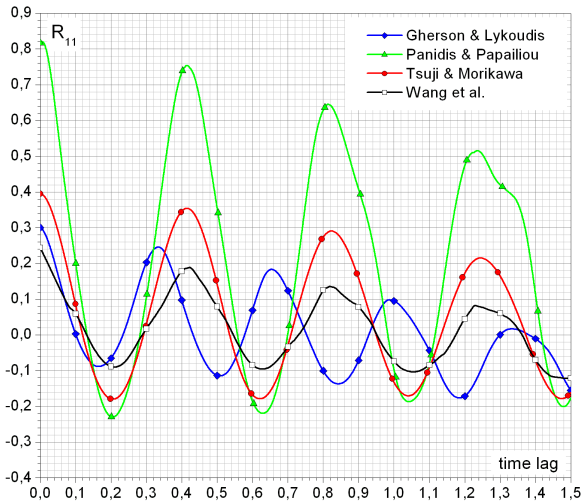

(c) $x_1 = 0.5$, $x_2 = 0.85$ and $x_3 = 0.25$

Figure 10: Autocorrelation functions evaluated at different span-wise positions in bubble-swarm flow using different methods for signal processing of temporal liquid velocity signals .

Table 3: Performance of different methods for signal processing in bubbly flows in predicting rms value of liquid velocity fluctuations

	bubble-train	bubble-swarm		
		x_2		
		0.25	0.5	0.85
u_{l1rms} [a]	0.3595	0.4165	0.5154	0.5479
TM [c b]	0.4459	0.4577	0.6367	0.5239
PP [d b]	0.3595	0.5321	0.8240	0.9038
GL [e b]	0.3595	0.4164	0.5154	0.5479
W [f b]	0.3200	0.3857	0.4843	0.4937

[a] computed from equation (15)
[b] autocorrelation function at zero time lag, $R_{11}(0)$
[c] Tsuji & Morikawa (1982)
[d] Panidis & Papailiou (2000)
[e] Gherson & Lykoudis (1984)
[f] Wang *et al.* (1990)

6 Analysis of energy spectra of liquid velocity fluctuations in computed bubble-array flows

The one-dimensional energy spectra of liquid velocity fluctuations in vertical (x_1) direction evaluated by taking the Fast Fourier Transformation of the aforementioned autocorrelation functions are shown in Figure 11 for the bubble-train flow and in Figure 12 for the bubble-swarm flow, both in log-log and in semi-log coordinates (inset graphics).

The lowest resolved frequency is in the case of bubble-train flow $\Omega = 0.6$ and $\Omega = 0.3$ in the bubble-swarm scenario. This difference arises from the following reason. In order to apply the Fast Fourier Transformation correctly, the number of sample points should be an integer power of 2. In that context, due to the longer period of steady state in the bubble-swarm than in the bubble-train flow scenario, the autocorrelation function could be evaluated along a longer time lag in the former case (note that in Figure 9 and 10 the whole length of considered time lag is not presented).

In order to determine the range of frequencies in which energy spectrum has physical significance, an attempt has been made to estimate Kolmogorov time scale. The dimensionless value of Kolmogorov time scale can be evaluated from:

$$\tau_K = u_{\text{ref}}^{1.5} l_{\text{ref}}^{-0.5} Re_{\text{ref}}^{-0.5} (\varepsilon^*)^{-0.5}, \qquad (20)$$

where ε^* is dissipation rate of liquid turbulence kinetic energy.

In this analysis the magnitude of ε^* has been adopted from Ilic (2006), where the liquid turbulence dissipation for the same configuration of bubble-array flows as considered here is evaluated on the basis of its rigorous mathematical formulation. It is, however, noted that doing so (i) the validity of Taylor hypothesis is assumed since in Ilic (2006) a space (along vertical lines) and not the time averaging is applied and (ii) that the spatial distribution of turbulence energy dissipation obtained by Ilic (2006) has been averaged to obtain one representative value.

The averaging is in the case of the bubble-swarm flow done over the whole channel domain, what resulted in $\varepsilon^* = 0.34 m^2/s^3$. With this value of the turbulence energy dissipation dimensionless Kolmogorov time scale of $\tau_K = 0.0857$ has been found. In relation the this, as the upper limit of physically meaningful turbulence energy spectrum, the dimensionless frequency of $\Omega_K = 1/\tau_K = 11.67$ has been set.

In the case of bubble-train flow, the averaging of spatially distributed turbulence energy dissipation over the whole channel has no physical background because the results show that all the turbulence kinetic energy of the liquid phase is fully dissipated in the flow region where the bubble rises. Performing the averaging over this part of the channel the mean value of the turbulence energy dissipation of $\varepsilon^* = 0.22 m^2/s^3$ has been evaluated, what gave an estimate of Kolmogorov time scale of $\tau_K = 0.1064$, i.e. something lower value of $\Omega_K = 1/\tau_K = 9.40$ than in the case of bubble-swarm flow.

Figures 11 and 12 show pronounced peaks in energy spectra evaluated for all the considered time signals and with all the applied methodologies. The magnitudes of frequencies at which these peaks appear are used as a criterium to validate the performance of different approaches for processing of defective liquid velocity signals in bubbly flows. The value of the frequencies at which the peaks in energy spectra appear should correspond to the time that a bubble needs to rise the height of the flow domain. Table 4 shows that the frequency of the peaks obtained applying methods of Tsuji & Morikawa (1982), Panidis & Papailiou (2000) and Wang *et al.* (1990) are in a good agreement with the frequency of bubble passage, $\overline{u}_{b1}^m/l$. On the other side, the frequencies corresponding to the peaks in the energy spectra evaluated by the method of Gherson & Lykoudis (1984) do not agree with the frequency imposed by the periodic boundary conditions in the rise direction. This result is to expect since in the method of Gherson & Lykoudis (1984) the gaps are not bridged over, but the liquid signals are simply patched together, what results in a shift of the spectrum peak toward higher frequencies. The amount of the frequency shift depends on the time-averaged gas volumetric fraction. The lower the time averaged gas volumetric fraction, the lower is the frequency shift. In this context, it can be concluded that the method of Gherson & Lykoudis (1984) can give acceptable results only for very low values of the temporal gas fraction. The results of the present investigation cannot provide definition of the maximal magnitude of the time averaged gas volumetric fraction for which the approach of Gherson & Lykoudis (1984) is valid, but it can be stated that it is lower than the lowest value of temporal gas fraction of $\approx 5\%$ considered here (see Figure 7).

Table 4: Estimation of frequencies of energy dominant eddies in investigated bubble-array flows.

	bubble-train	bubble-swarm		
		x_2		
		0.25	0.5	0.85
$\overline{u}^m_{b1}/l$ [a]	3.59	2.03	2.35	2.31
$\sqrt{2k_l}/d_b$	1.46	2.16	2.41	2.40
TM[b] PP[c] W[d]	3.66	2.14	2.44	2.44
GL[e]	4.27	2.44	2.75	3.05

[a] $\overline{u}^m_{b1}$ is the mean value of the rise velocity of m^{th} bubble (see Figure 4) over here considered time averaging interval
[b] Tsuji & Morikawa (1982)
[c] Panidis & Papailiou (2000)
[d] Wang *et al.* (1990)
[e] Gherson & Lykoudis (1984)

Table 5: Performance of different methods for signal processing in bubbly flows in predicting kinetic energy of liquid velocity fluctuations in vertical direction.

	bubble-train	bubble-swarm		
		x_2		
		0.25	0.5	0.85
$u^2_{l1rms}/2$ [a]	0.0646	0.0867	0.1328	0.1501
TM [c b]	0.2109	0.1018	0.2379	0.2746
PP [d b]	0.1496	0.1328	0.3637	0.6087
GL [e b]	0.0890	0.0926	0.1779	0.18726
W [f b]	0.0981	0.0659	0.1262	0.1494

[a] u_{l1rms} computed from equation (15)
[b] computed as l.h.s. of equation (21)
[c] Tsuji & Morikawa (1982)
[d] Panidis & Papailiou (2000)
[e] Gherson & Lykoudis (1984)
[f] Wang *et al.* (1990)

Finally, Table 4 shows, that in the case of the bubble-swarm flow the frequencies at which peaks in the energy spectra occur can be very well predicted if turbulence scales are expressed in the following way: velocity scale evaluated from liquid turbulence kinetic energy ($\sqrt{2k_l}$) and length scale adopted to be equivalent bubble diameter (d_b). It is, however, noted that, this way has not given good predictions of frequency of energy dominant eddies in bubble-train flow.

As the next criterion for the performance of different methods for signal processing in bubbly flows, the energy content of the reconstructed signal is considered. In this context, the fulfillment of the following property of one-dimensional energy spectra (Davidson (2004)):

$$\int_0^\infty F_{11}(\Omega)d\Omega = \frac{1}{2}u^2_{l1rms}, \qquad (21)$$

by the four different methods is put into consideration. It is, however, noted that the integral in the above equation is evaluated up to the frequency corresponding to the Kolmogorov time scale. The results presented in Table 5 show that all but the method of Wang *et al.* (1990) overestimate turbulence energy of the liquid phase. The highest overestimation is obtained by the method of Panidis & Papailiou (2000) followed by the method of Tsuji & Morikawa (1982). On average, the methods of Gherson & Lykoudis (1984) and Wang *et al.* (1990) give similar discrepancy in estimation of the liquid turbulence energy, what is not surprising since Wang *et al.* (1990) gap the signal by the mean value so that the energy should have similar value as in the patched signal of Gherson & Lykoudis (1984).

Finally, in Figure 12 it can be seen that there is a range of frequencies for which turbulence energy spectra in log-log plot show a constant slope of -1 for all four methods. This value is significantly different from $-5/3$ or $-8/3$ usually reported as the slope of the energy spectra in bubbly flows. It is, however, recalled that the present paper deals with pure bubble-induced so-called pseudo turbulence, where any significant shear is not present. Especially due to the absence of the shear one may not expect an inertial subrange with a spectral slope close to $-5/3$. This result is, further, in accordance with the theoretical considerations of Lance & Bataille (1991), who reported the slope of the power spectrum at low wave numbers of -1 for bubbly flows in which the pseudo-turbulence is dominant.

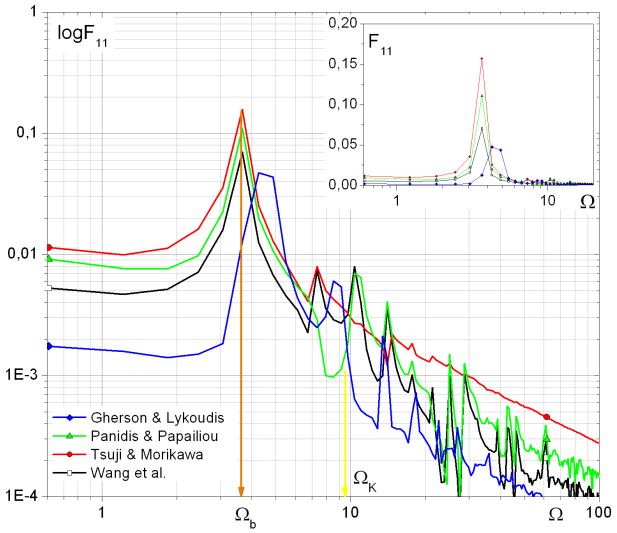

Figure 11: Axial turbulent energy spectra evaluated for bubble-train flow.

Conlusions

This paper presents investigations of liquid velocity fluctuations due to the presence of bubbles and their relative motion. The investigations are based on direct numerical simulations of liquid flows driven by monodisperse bubble-arrays. The goal of the performed work was to shed some light on the structure and dynamics of turbulence in gas-liquid flows through evaluation and analysis of the time / space correlations of the fluctuating velocity field in the continuous liquid phase.

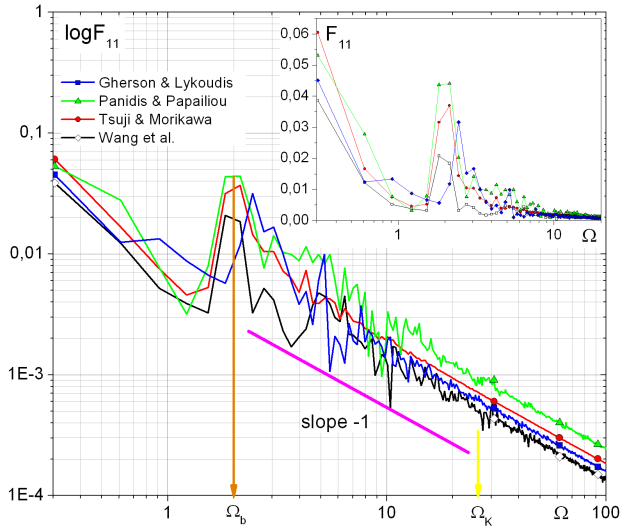

(a) $x_1 = 0.5$, $x_2 = 0.25$ and $x_3 = 0.25$

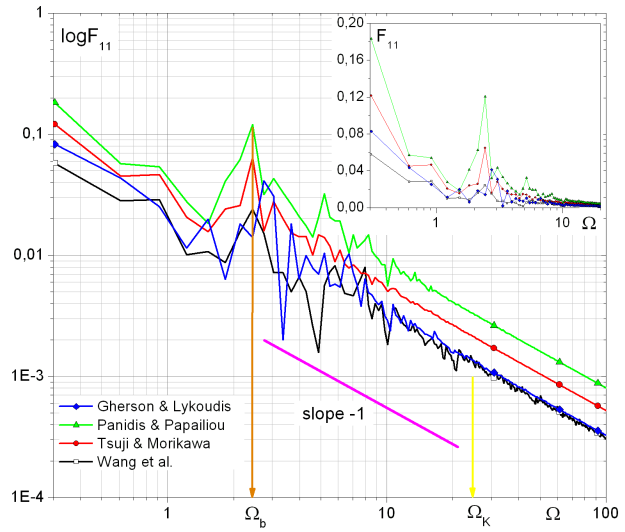

(b) $x_1 = 0.5$, $x_2 = 0.5$ and $x_3 = 0.25$

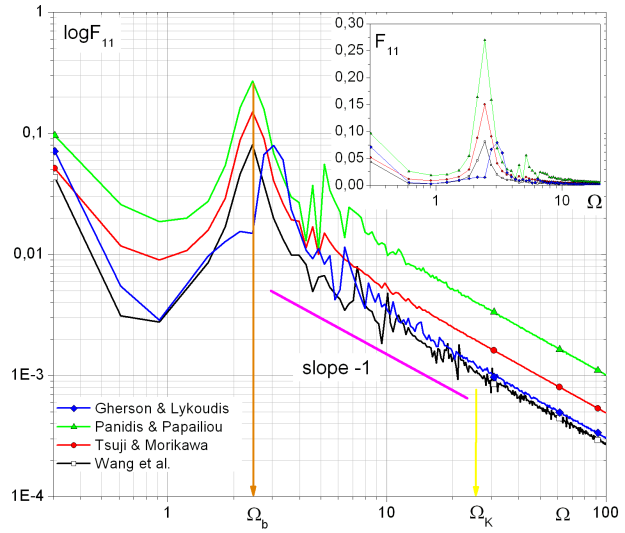

(c) $x_1 = 0.5$, $x_2 = 0.85$ and $x_3 = 0.25$

Figure 12: Axial turbulent energy spectra evaluated at different span-wise positions for bubble-swarm flow

In particular, attention has been paid to performance of different approaches for bridging over the gaps in the liquid velocity signal due to bubble passages.

The method of Gherson & Lykoudis (1984) where the liquid velocity signals are patched together and the gaps due to bubble passage are removed does not give correct frequency of the most energetic turbulence scales. This frequency is overestimated and the amount of overestimation depends on the mean temporal gas fraction at the sensor position. The method can, therefore, not be recommended in general, but only for very low gas contents. The methods of Panidis & Papailiou (2000) and of Tsuji & Morikawa (1982) give the correct frequency of energy spectrum peak, but overestimate the energy of the signal. Finally, the method proposed by Wang *et al.* (1990) seems to be the most promising one, since it was able to predict correct frequency of energy spectrum peak and to give reasonable predictions of the energy content of the liquid velocity fluctuations.

In the present simulations, the intensity of the pseudo-turbulence is rather small. It was, therefore, not a goal to make statements regarding the slope of the one-dimensional power spectrum at high frequencies. However, it is interesting to note that always a slope of -1 is found which is in agreement with the theoretical considerations of Lance & Bataille (1991) for flows dominated by pseudo-turbulence.

Nomenclature

a_i	interfacial area concentration
d	diameter
Eo	Eotvos number
f	liquid volumetric fraction
F_{11}	Turbulent energy spectrum
g	gravitational acceleration
$\mathbf{g}$	gravity vector
l	length
M	Morton number
n	number of bubbles in domain
$\mathbf{n}$	unit normal vector at phaase interface
p	pressure
$\mathbf{r}$	position vector to bubble center-of-mass
R_{11}	Autocorrelation function
Re	Reynolds number
t	time
$\mathbf{u}$	velocity
V	volume
We	Weber number
x_1, x_2, x_3	Cartesian coordinates
$\mathbf{x}$	position vector

Greek letters

α	volume fraction
Γ_ρ	Gas-to-liquid density ratio
Γ_μ	Gas-to-liquid viscosity ratio
κ	interface curvature
μ	dynamic viscosity
ρ	density

σ	coefficient of surface tension
Ω	frequency

Subscripts

1,2,3	coordinate indices
b	bubble
g	gas
i	interface
l	liquid
ref	reference value

Superscripts

*	dimensional quantity
m	bubble index

References

Cui, Z. & Fan, L.S. Turbulence energy distribution in bubbling gas-liquid and gas-liquid-solid flow systems. Chem. Eng. Sci., Volume 59, 1755 – 1766 (2004)

Cui, Z. & Fan, L.S. Energy spectra for interactive turbulence fields in a bubble column. Ind. Eng. Chem. Res. Sci., Volume 44, 1150 – 1159 (2005)

Davidson, P.A. Turbulence An Introduction for Scientists and Engineers. Oxford University Press (2004)

Gherson, P. & Lykoudis, P.S. Local measurements in two-phase liquid-metal magneto-fluid-mechanistic flow. J. Fluid Mech., Volume 147, 81 – 104 (1984)

Harteveld, W.K., Mudde, R.F. & Van den Akker, H.E.A. Estimation of turbulence power spectra for bubbly flows from Laser Doppler Anemometry signals. Chem. Eng. Sci., Volume 60, 6160 – 6168 (2005)

Ilic, M., Wörner, M. & Cacuci, D.G. Balance of liquid-phase turbulence kinetic energy equation for bubble-train flow. Journal of Nuclear Science and Technology, Volume 41, 331 – 338 (2004)

Ilic, M., Wörner, M. & Cacuci, D.G. Investigations of liquid phase turbulence based on direct numerical simulations of bubbly flows. Proc. NURETH 11, Avignon, France, October 2-6 (2005)

Ilic, M., Statistical analysis of liquid phase turbulence based on direct numerical simulations of bubbly flows, Ph.D. Thesis, University Karlsruhe (2006)

Kataoka, I. & Serizawa, A. Basic equations of turbulence in gas-liquid two-phase flow. Int. J. Multiphase Flow, Volume 15, 843 – 855 (1989)

Lance, M. & Bataille, J. Turbulence in the liquid phase of a uniform bubble air-water flow. J. Fluid Mech., Volume 222, 95 – 118 (1991)

Luther, S., Rensen, J., van den Berg, T.H. & Lohse, D. Data analysis for hot-film anemometry in turbulent bubbly flow. Exp. Thermal Fluid Sci., Volume 29, 821 – 826 (2005)

Mudde, R.F., Groen, J.S. & van den Akker, H.E.A. Liquid velocity field in a bubble column: LDA measurements. Chem. Eng. Sci., Volume 52, 4217 – 4224 (1997)

Panidis, T. & Papailiou, D.D. The Structure of two-phase grid turbulence in a rectangular channel: an experimental study. Int. J. Multiphase Flow, Volume 26, 1369 – 1400 (2000)

Rensen, J., Luther, S. & Lohse, D. The effects of bubbles on developed turbulence. J. Fluid Mech., Volume 538, 153 – 187 (2005)

Sabisch, W., Wörner, M., Groetzbach, G. & Cacuci, D.G. 3D volume-of-fluid simulation of a wobbling bubble in a gas-liquid system of low Morton number. Proc. of 4^{th} International Conference on Multiphase Flow, New Orleans, USA (2001)

Shawkat, M.E., Ching, C.Y. & Shoukri, M. On the liquid turbulence energy spectra in two-phase bubbly flow in a large diameter vertical pipe. Int. J. Multiphase Flow, Volume 33, 300 – 316 (2007)

Tsuji, Y. & Morikawa, Y. LDV measurements of an air-solid two-phase flow in a horizontal pipe. J. Fluid Mech., Volume 120, 385 – 409 (1982)

Wang, S.K., Lee, S.J., Jones, O.C. & Lahey, R.T. Jr. Statistical Analysis of Turbulent Two-Phase Pipe Flow. J. Fluids Eng. Volume 112, 89 – 95 (1990)

Wörner, M. Invariance of the velocity field induced by a bubble rising steadily through liquid under variation of the gas-liquid density ratio. Proc. of German-Japanese Workshop on Multiphase Flow, Karlsruhe, Germany, (2003). Wissenschaftliche Berichte Forschungszentrum Karlsruhe, FZKA 6759, pp. G10-G21 (2003) (http://bibliothek.fzk.de/zb/berichte/FZKA6759.pdf)

Zenit, R., Koch, D.L. & Sangani A.S. Measurements of the average properties of a suspension of bubbles rising in a vertical channel. J. Fluid Mech., Volume 429, 307-342 (2001)